LIGO SURF Progress Report: Studying the effects of higher-order modes on the parameter estimation of precessing low-mass binary black holes

Rupini V. Kamat,[1] Patricia Schmidt,[2] Rory Smith,[2] and Yanbei Chen[2]

[1]*LIGO SURF Student, California Institute of Technology*
[2]*LIGO SURF Mentors, California Institute of Technology*

(Dated: July 6, 2016)

I. BACKGROUND INFORMATION

LIGO, the Laser Interferometer Gravitational-Wave Observatory, has recently made a huge breakthrough in the field of gravitational wave (GW) astronomy with the first ever detection of gravitational waves [1]. The observed waves were generated by a merging binary black hole system with a total mass of about $70M_{\odot}$ [2]. As theoretically predicted, the detected GW signal evolved in three stages: the inspiral, the merger, and the ringdown.

The inspiral stage of a black hole binary's evolution is characterized by a large separation of the binary and orbital speeds much smaller than the speed of light. Because the motion of the binary is non-relativistic during the inspiral phase, the binary dynamics and the inspiral waveform can be calculated by expanding the Einstein field equations in terms of v/c using post-Newtonian formalism. However, as gravitational waves carry angular momentum and orbital energy away from the system, the orbit of the binary decays, the separation of the binary becomes small, and the speeds of the black holes approach the speed of light. At these speeds, the non-linearity of General Relativity becomes significant, and the waveform must be calculated using the numerical solution to the relativistic two-body problem, or numerical relativity. Finally, after the binary black holes merge into a single black hole, the system enters its ringdown stage, which corresponds with the quasi normal modes emitted by the perturbed black hole until it "settles down" to the stationary Kerr solution for spinning black holes. The waveform emitted during the ringdown stage of the binary's evolution must either be calculated using numerical relativity or via perturbation theory.

Because gravitational waves are very weak, compact binary coalescences, such as the merger of two black holes, are among the few systems that can currently be observed by LIGO. Nonetheless, the gravitational waveforms of these objects encode a large amount of information about each system that would otherwise be inaccessible, as systems like binary black holes are not thought to be observable through electromagnetic astronomy. Thus, the gravitational waveforms of these systems can help us answer astrophysically interesting questions, for example how compact binaries are formed, what are the masses and spins of objects in compact binaries, how they evolve in time, and how these types of systems are distributed in space.

However, while LIGO has now proven that it is capable of detecting gravitational waves from these astronomical sources, our ability to use observed gravitational waveforms to analyze the properties of the systems they originated from is still relatively limited. This may be due to a number of factors, including the fact that many of the currently used waveform models use the quadrupole approximation [13]. This approximation may lead to parameter degeneracies that prevent us from conclusively determining the physical parameters of an observed system. Such degeneracies include the spin-mass ratio degeneracy, the orientation-distance degeneracy, and many more. For example, Figures 3 and 4 in [3] illustrate the spin-mass degeneracy for binary black holes.

Thus, in order for us to begin to use gravitational-wave observations to answer astronomically interesting questions, we must first improve our ability to probe the properties of the systems we observe. One potential

way to break parameter degeneracies and thus improve our parameter estimation abilities is the inclusion of higher modes in our theoretical waveforms [4, 5]. While the quadrupole approximation may be sufficient for highly symmetric binaries, binary systems that contain asymmetries, such as unequal mass ratios and unequal spins, emit a significant amount of gravitational-wave energy in higher modes, as, for example, shown in Figures 1 and 2 in [6]. Thus, higher modes carry a significant amount of information about the source system, and the inclusion of higher modes in template waveforms has the potential to allow us to recover large amounts of information from an observed waveform.

II. PROJECT DESCRIPTION

We propose that including higher-order modes in our template waveforms has the potential to break parameter degeneracies, thus allowing us to more accurately recover the properties of an observed system through its detected gravitational waveform. Similar work has been done by O'Shaughnessy et al. [4, 7], who analyzed the inspiral waveforms of select black hole–neutron star binary systems to investigate the possibility of breaking some of these parameter degeneracies. O'Shaughnessy et al. found that for the fiducial system they analyzed, the inclusion of higher order modes broke degeneracies regarding the direction of the system's angular momentum, but otherwise had little impact on the estimation of the systems' parameters.

Our goal in this project is to extend this analysis to a range of precessing binary black hole systems to systematically assess what impact higher order modes have on parameter estimation for the systems we will consider. In particular, we will be analyzing precessing, low-mass binary black holes with various spin configurations and a total mass of less than $12M_{\odot}$. We will not analyze systems with higher total masses, as we will only be considering inspiral waveforms, and for black hole binaries with a total mass $\geq 12M_{\odot}$, the merger phase appears in the LIGO band. Using pure inspiral waveforms for such system may result in biased results during parameter estimation [8], hence the restricted analysis. While it is expected that the effects of higher modes will be more significant during the merger phase than during the inspiral phase, we do not currently have NR models for the merger waveforms of precessing binary black holes that would enable us to study these effects, which is why our analysis will be limited to inspiral waveforms.

III. APPROACH

First, we construct a set of model precessing low-mass black hole binaries to analyze. In addition to the total mass constraint of $\leq 12M_{\odot}$ mentioned previously, we construct our binary cases by choosing systems which we would expect to emit a significant amount of radiation in higher modes. We then generate the gravitational waveforms produced by these systems, including higher modes. For our higher modes analysis, we will be using the post-Newtonian waveforms for precessing binary black holes as given in Appendix A in [9].

We then analyze the resulting simulated waveforms in two stages: first using Fisher analysis and then using full Markhov Chain Monte Carlo (MCMC) parameter analysis for select cases. We use Fisher analysis to get a best estimate of the improvement in parameter uncertainty, if any, that results from the inclusion of higher waveforms. We then isolate the binary cases for which the inclusion of higher modes results in the most improvement in parameter estimation, according to our Fisher analysis, and perform full MCMC parameter estimation runs to more thoroughly quantify the effects that including higher modes has on parameter estimation.

A. Fisher Matrix Analysis

Due to the high computational cost of a full MCMC parameter estimation analysis, we have decided to begin our analysis of the effects of higher modes on parameter estimation with a Fisher information matrix analysis. The Fisher information matrix is a tool that allows one to measure the amount of information that a given set of data provides about some unknown parameter that can be used to model the data set. It is defined as follows:

$$\Gamma = -[\nabla\nabla \ln(L)] \tag{1}$$

where L is the likelihood function described in Sec. III B. The inverse of the Fisher matrix then gives the covariance matrix of the posterior probability distribution, where the statistical uncertainty of a measured parameter λ_i due to noise is given by

$$(\Delta\lambda_i)_{\text{stat}} = \sqrt{\Gamma^{-1}_{ii}} \tag{2}$$

and the remaining entries in the matrix $\Gamma_{ij} = \Gamma_{ji}$ give the correlation between two parameters λ_i and λ_j. An example of this is shown in Appendix A. Patricia: What does of this mean? State more clearly what is shown in the appendix.

In the case of a gravitational wave signal, we can assume that an observed signal $s \in \mathbb{R}$ contains some noise n and a gravitational wave signal $h_0(\vec{\lambda}_{\text{true}})$, where $\vec{\lambda}_{\text{true}}$ are the true parameters of the observed system.

$$s = n + h_0(\vec{\lambda}_{\text{true}}) \tag{3}$$

Thus, if we model the signal as $h(\vec{\lambda})$, we can represent the likelihood function as the following:

$$L(s|\vec{\lambda}) \propto e^{-\langle s-h(\vec{\lambda}), s-h(\vec{\lambda})\rangle/2} \tag{4}$$

where $\langle h, g\rangle$ is the noise-weighted inner product of two real-valued functions h and g, as defined below:

$$\langle h, g\rangle = 4\text{Re}\int_0^\infty \frac{\tilde{h}(f)\tilde{g}^*(f)}{S_n(f)} df, \tag{5}$$

where the $\tilde{h}(f)$ is the Fourier transform of the function into the frequency domain, $\tilde{g}^*(f)$ is the complex conjugate of $\tilde{g}(f)$, and $S_n(f)$ is the one-sided noise power spectral density (PSD) of the LIGO detector. From Eq. 5 we define the norm of a waveform as

$$||h|| = \sqrt{\langle h, h\rangle} \tag{6}$$

If we use that the noise is Gaussian with a mean of zero and that our prior probability distribution for the data is a flat distribution, the elements of the Fisher information matrix are given by:

$$\Gamma^{ij}(\vec{\lambda}) = \langle \frac{\partial h}{\partial \lambda_i}(\vec{\lambda}), \frac{\partial h}{\partial \lambda_j}(\vec{\lambda})\rangle, \tag{7}$$

Thus, if h is an accurate model for the system's true waveform h_0, the posterior probability distribution, or the probability distribution of parameters that would result from a thorough parameter estimation analysis, can then be approximately described by the *maximum likelihood estimate* $\vec{\lambda}'$, i.e. the set of parameters that maximize $L(s|\vec{\lambda})$.

Suppose, however, that the model waveform h is different from the true waveform h_0, such that

$$\delta h(t;\vec{\lambda}) = h_0(t;\vec{\lambda}) - h(t;\vec{\lambda}) \neq 0 \tag{8}$$

Then, the maximum likelihood estimate $\vec{\lambda}'$ for the true parameters has some systematic error that is not described by Eq. 2, which quantifies only the statistical error due to the noise. Using the derivation shown in Section 2.3.3 of [10], we find that the systematic error that arises from an incomplete waveform model is given by:

$$(\Delta\lambda_i)_{\rm sys} = [\Gamma^{-1}(\vec{\lambda}')]_{ij} \, \langle \delta h_0(\vec{\lambda}'), \frac{\partial h}{\partial \lambda_j}(\vec{\lambda}') \rangle \tag{9}$$

The total error in the estimate for a single parameter is given by the sum of the statistical error and the systematic error. Because systematic error is independent of signal strength, it is the dominant source of parameter estimation error at high signal-to-noise ratio (SNR), but becomes negligible compared to statistical error at low SNR. Patricia: Quantify this statement. SNR is a detection statistic which quantifies signal strength and is defined as follows:

$$\rho = \max_{\lambda} \langle s, \hat{h}(\lambda) \rangle, \tag{10}$$

where s is the observed signal and $\hat{h}$ is the normalized version of the template waveform used to model the data.

$$\hat{h}(\vec{\lambda}) = \frac{h(\vec{\lambda})}{||h||} \tag{11}$$

Thus, we can define some SNR-dependent "indistinguishability criterion" to determine whether or not two different waveforms h and h_0 can be considered *indistinguishable* from one another. Following [11], we call two waveforms indistinguishable if $(\Delta\lambda)_{sys} < (\Delta\lambda)_{stat}$. Thus, we can use Fisher matrices to analyze whether or not the quadrupole and $\ell = 2$ waveforms of a system are "indistinguishable" from the higher-mode-inclusive waveform, hereafter referred to as the "full waveform", of the same system. This enables us to determine if there exist areas in the parameter space for low mass, precessing binary black holes where significant systematic error arises from using only quadrupole or all $\ell = 2$ waveforms during parameter estimation. Once we have isolated these areas in the parameter space, we can chose a selection of binary black hole cases on which to perform a full parameter estimation analysis.

B. Bayesian Analysis

Having chosen our binary cases using a Fisher information matrix analysis, full parameter recovery on a few selected cases will be performed twice: once using the quadrupole waveforms as template waveforms and once again using the full waveforms. This will enable us to compare the results from each parameter estimation run and study the effects of including higher modes.To measure the source parameters, we will

be performing a *Bayesian analysis* using the tools offered in the LALInference software library for Bayesian parameter estimation [12].

In general terms, the process of Bayesian analysis is as follows. First, a probability distribution, known as the *prior distribution* and represented as $p(\vec{\lambda})$, is constructed for each set of parameters $\vec{\lambda}$ in the binary parameter space. Each set of parameters in the binary parameter space includes values like component masses, spins, position on the sky, distance to the source, orientation of the binary, and many more. The prior distributions we will use in our project consist of uniform distributions over a given range for parameters like component masses and spin magnitudes, and isotropic distributions over the unit sphere for the spin orientation.

After a prior distribution has been constructed, the likelihood $L(s\,|\,\vec{\lambda})$ of the observed signal s given the parameters $\vec{\lambda}$ is calculated. Then, we multiply the likelihood function by the prior distribution $p(\vec{\lambda})$ and normalize by $p(s)$, the probability of the signal independent of the distribution of the parameters also known as the evidence. This gives us the posterior probability distribution, $p(\vec{\lambda}\,|\,s)$, as described by Bayes' Theorem:

$$p(\vec{\lambda}\,|\,s) = \frac{L(s\,|\,\vec{\lambda})\,p(\vec{\lambda})}{p(s)} \tag{12}$$

The parameter estimate is then given by the median value of the posterior distribution, and the error is given by the values that correspond to the 90% credible interval, or the parameter values that enclose 90% of the probability of the distribution. We will then compare the results of the two parameter estimation runs for each binary case, and analyze how the inclusion of higher modes affects our ability to accurately constrain the parameters of the model system. This will enable us to determine whether or not the inclusion of higher modes facilitates the breaking of parameter degeneracies in the inspiral case.

IV. CURRENT STATUS OF RESULTS

A. Visualization of the gravitational radiation field

The gravitational radiation field of a binary black hole can be decomposed into a set of gravitational-wave modes, $h_{\ell m}$, in a basis of spin-weighted spherical harmonics. We can write the full waveform of a system of binary black holes as:

$$h(t,\vec{\lambda};\theta,\phi) = \sum_{\ell=2}^{\infty}\sum_{m=-\ell}^{\ell} h_{\ell m}(t,\vec{\lambda})\;{}^{-2}Y_{\ell m}(\theta,\phi), \tag{13}$$

where (θ,ϕ) denote the angles on the unit sphere. In particular, θ is the inclination angle the total angular momentum vector $\vec{J}_0$ of the binary and the observer, and ϕ is the corresponding azimuthal angle in the binary source frame; $h_{\ell m}(t,\vec{\lambda})$ is the amount of radiation emitted in a given mode (defined by the values of ℓ and m) as a function of time and the binary parameters $\vec{\lambda}$, and ${}^{-2}Y_{\ell m}(\theta,\phi)$ are the spin-weighted spherical harmonic modes.

Thus, using the $h_{\ell m}(t,\vec{\lambda})$ equations given in Appendix A of [9], we can use Eq. 13 to construct the projection of the gravitational radiation field of a given system onto the unit sphere at various points in time. In doing so, we generated a set of animations showing the time evolution of the radiation emitted by a precessing black hole binary during its inspiral phase.

The first animation included only the quadrupole modes, $(l=2, m=\pm 2)$, the second included all $(\ell=2)$-modes, and the last included all $(\ell=2)$- and all $(\ell=3)$-modes. The system we used had the following parameters $\vec{\lambda}$: a mass ratio of $q=m_1/m_2=4$, an initial separation of $a_0=50M$, and dimensionless spin vectors of $\vec{\chi}_1=(0.9,0,0)$ and $\vec{\chi}_2=(0,0.9,0)$.

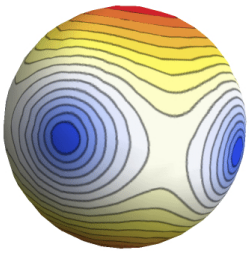

(a) $\ell = 2$ modes at $t = 1000$

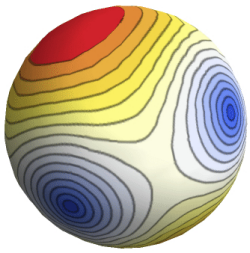

(b) $\ell = 2$ modes at $t = 7000$

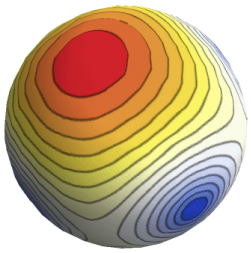

(c) $\ell = 2$ modes at $t = 12000$

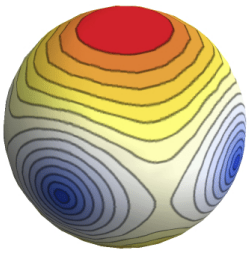

(d) quadrupole modes at $t = 1000$

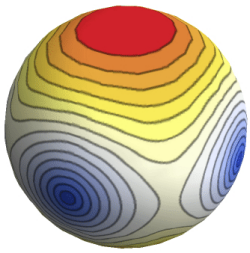

(e) quadrupole modes at $t = 7000$

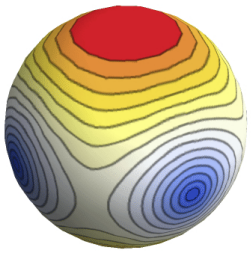

(f) quadrupole modes at $t = 12000$

FIG. 1: The top panel ((a)-(c)) shows the radiation field projected onto the unit sphere for three different times during the time evolution of the entire $\ell = 2$ waveform emitted by a black hole binary system, while the bottom panel ((d)-(f)) displays still frames from an animation of the quadrupole-only waveform of the same system for the same times.

The purpose of this was to visualize how the radiation field of a black hole binary system changes with the inclusion of higher modes. This enables our understanding of just how much information is carried by the higher modes of a system's gravitational radiation field.

Frames from two time evolutions are shown in Fig. 1. The top panel correspond with the animation of the $(\ell = 2)$-modes, and the bottom images correspond with the animation of the quadrupole modes.

We know that a binary emits gravitational radiation most strongly in the direction of the orbital angular momentum of the system. In Fig. 1, the red hotspot indicates the maximum emission at any given time. Similarly, we know that a binary black hole system emits the least amount of radiation in the orbital plane. Thus, the location of the blue coldspots in each image indicates the position of the orbital plane of the system at various points in time.

With this information, we can see that the images corresponding with the full $\ell = 2$ waveform of the system show a tilt of the orbital angular momentum vector with respect to the total angular momentum vector of the system, which is directed along the z-axis. They clearly show that as time goes on the orientation of the binary changes due to precession. The frames in the bottom panel however, show very little tilt of the orbital plane and no visible precession of the binary. These distinctions were displayed even more clearly in the animated versions of the frames above. Ultimately, we found that the time evolution of the quadrupole waveform of the system looks almost like the waveform of an aligned spin system, with very little visible

precession, while the entire $l = 2$ waveform of the system shows clear and significant precession. Hence, the exclusion of the non-quadrupolar $(\ell = 2)$-modes leads to a significant loss of information about the binary which is directly reflected into the waveforms as illustrated in Fig. 3.

The differences between the $\ell = 2$ inclusive waveform and the $\ell = 3$ inclusive waveform (i.e. a slight increase in the magnitude of the oscillations in size of the "hotspot" on the contour map) were less visually dramatic, but nonetheless indicated that important information about the dynamics of the binary is carried by the $\ell = 3$ mode of the binary's waveform.

Ultimately, these animations allow us to get a better visual understanding of the effect that including higher modes has on the waveform of a system. While this may not necessarily translate directly to a bias in parameter estimation, it helps us visualize just how much information is really carried by the higher modes of a system's waveform.

B. Matches

In order to determine areas in the parameter space where we can expect to find large differences between the quadrupole waveform and the higher-mode-inclusive waveform of a given system, we examine the *match* between the two waveforms. The match is defined as the normalized inner product of two waveforms, maximized over phase and time shift, and is commonly used as a measure of similarity between two waveforms:

$$\mathscr{M}(h_1,h_2) = \max_{\Delta t,\Delta\Phi} \langle \frac{h_1}{||h_1||}, \frac{h_2}{||h_2||} \rangle = \max_{\Delta t,\Delta\Phi} \frac{2}{||h_1||||h_2||} \int_{-\infty}^{\infty} \frac{\tilde{h}_1(f)\tilde{h}_2^*(f)}{S_n(|f|)} df \tag{14}$$

Two waveforms that are exactly the same have a match of 1, while waveforms that are orthogonal have a match of 0. Thus, we can calculate the match between waveforms at various spins, mass ratios, values of (θ,ϕ), etc. to identify areas in the parameter space where the quadrupole waveform does not match well with the full waveform of the system. For example, Fig. 2 shows the match between the quadrupole waveform and the full $\ell = 2$ waveform of a black hole binary system with a total mass of $M = 12M_\odot$, an initial separation of $a_0 = 40M$, dimensionless spin vectors of $\vec{\chi}_1 = (0.9,\ 0,\ 0)$ and $\vec{\chi}_2 = (0,\ 0.9,\ 0)$, and an azimuthal angle of $\phi = 0$, at various inclination angles θ and at four different mass ratios, $q \in [1,2,3,4]$.

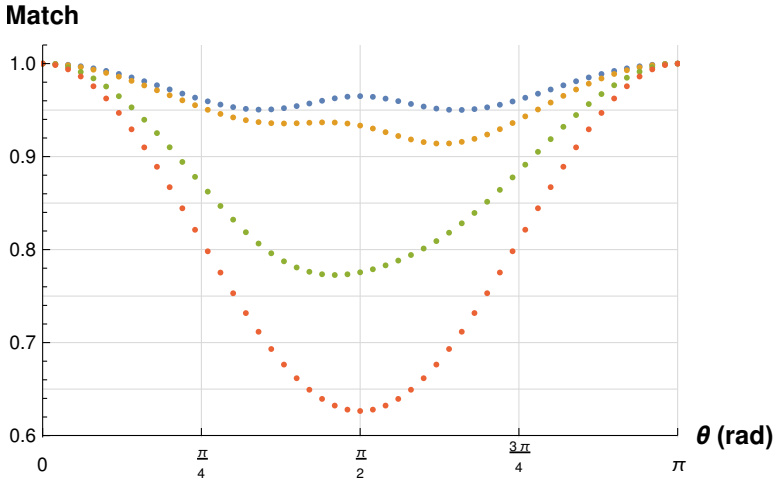

FIG. 2: The match between the quadrupole and $l = 2$ waveforms as a function of θ. The blue dots correspond to $q = 1$, the orange dots correspond to $q = 2$, the green dots correspond to $q = 3$, and the red dots correspond to $q = 4$.

We see that for each mass ratio, there exist values for the inclination angle θ where the match between the quadrupole waveform and the full $\ell = 2$ waveform dips well below 1. These dips are most pronounced for higher mass ratios. For example, the match between the $q = 4$ quadrupole and $\ell = 2$ waveforms drops by more than 35% from $\mathscr{M} = 1$ at $\theta = 0$ to $\mathscr{M} = 0.626$ at $\theta = \pi/2$. This indicates that, as anticipated, for more asymmetric systems, such as systems with higher mass ratios, there are significant differences between the system's quadrupole waveform and its higher mode-inclusive waveform.

To illustrate the differences between the quadrupolar and the higher modes waveform, we show the amplitudes of the waveforms in Fig. 3 for $q = 4$, $\vec{\chi}_1 = (0.9,\ 0,\ 0)$, $\vec{\chi}_2 = (0,\ 0.9,\ 0)$, and $a_0 = 40M$ system at the viewing angle $\theta = \pi/2$ and $\phi = 0$. We see that the low match between the two waveforms is reflected in the significant amplitude and phase difference between the actual signals.

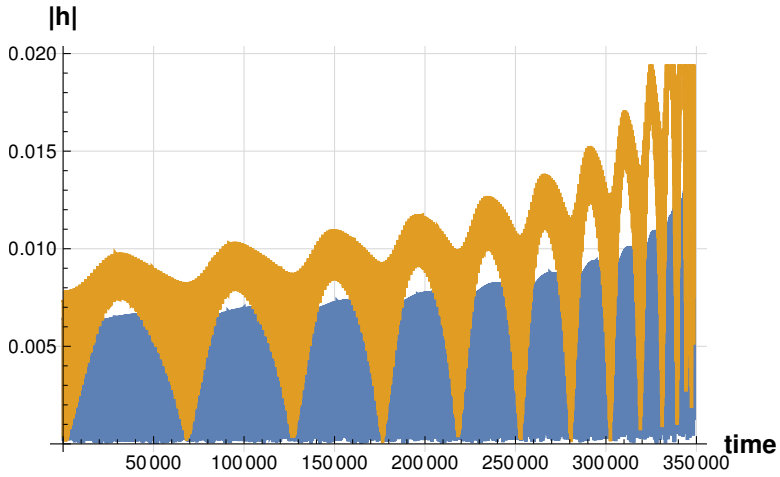

FIG. 3: The quadrupole (shown in blue) and $l = 2$ (shown in orange) waveform signals of a single black hole binary system at the inclination angle θ at which the match between the two waveforms is minimized

We then considered the match between the $\ell = 2$ waveform and the $\ell = 4$ waveform (which includes all $\ell = 2$, $\ell = 3$, and $\ell = 4$ modes) for the same system, and found that the match remains relatively close to 1 for most orientations, as shown in Fig. 4.

Although there is some mismatch between the waveforms, particularly at $\theta = \pi/2$, it is nowhere near as dramatic as the mismatch between the quadrupole waveform and the full $\ell = 2$ waveform. This tells us is that, as expected, the $\ell = 3$ and $\ell = 4$ modes of the precessing binary black hole system are subdominant to the $\ell = 2$ modes. Again, while the matches we calculated for the different waveforms do not necessarily translate directly to a bias in parameter estimation, they do allow us to gain a better understanding of what areas in the parameter space we can expect to find a large difference in the information that can be extracted from a quadrupole or $\ell = 2$ waveform as opposed to from an $\ell = 3$ or $\ell = 4$ waveform.

By holding $a_0 = 40M$ and $M = 12M_\odot$ constant and stepping through the remaining parameters (mass ratio, spin magnitudes, spin orientations, and inclination angle) in a systematic way, we were able see how the match between the $\ell = 2$ waveform and $\ell = 4$ waveform changes as a function of each parameter. For example, we saw that the match between the two waveforms is smallest for systems with parallel spins, i.e., $\vec{\chi}_i = (\chi_i, 0, 0)$. This is shown in Fig. 5, which displays the match between the $\ell = 2$ and $\ell = 4$ waveforms for $M = 12M_\odot$, $\vec{\chi}_1 = (0.6,\ 0,\ 0)$, $\vec{\chi}_2 = (0.6,\ 0,\ 0)$, and $a_0 = 40M$ as a function of θ. It is apparent that the minimum matches reached by this system for each mass ratio q are smaller than the minimum matches reached by the systems shown in Fig. 4.

Using our calculated matches, we were able to determine that the systems with the highest mismatch between the $\ell = 2$ and the $\ell = 4$ waveforms had approximately the following parameters: $q = 6$, $\vec{\chi}_1 = \vec{\chi}_2 = (0.6,\ 0,\ 0)$, and $\theta = \pi/2$.

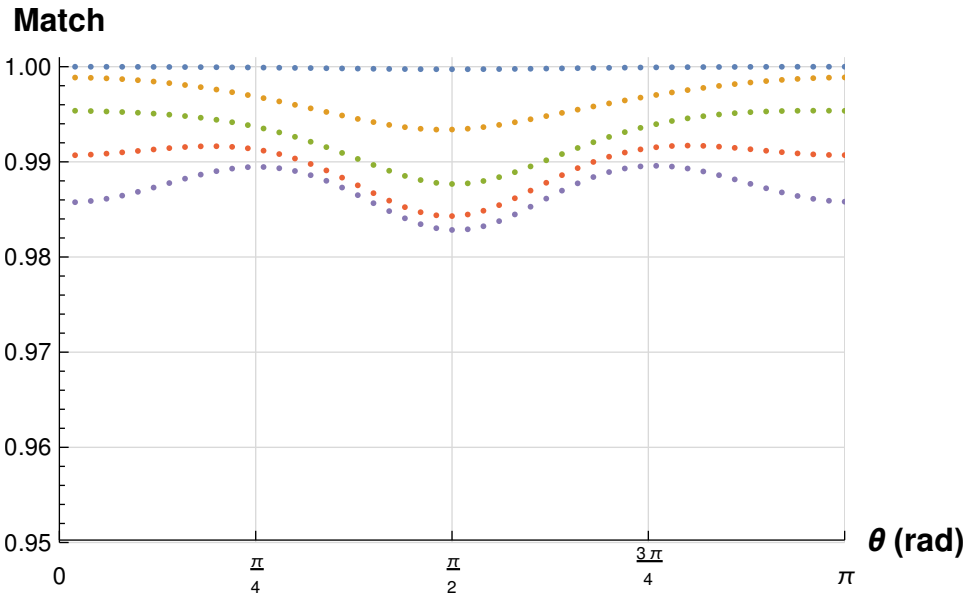

FIG. 4: The match between the $l = 2$ and $l = 4$ waveforms as a function of θ. The blue dots correspond to $q = 1$, the orange dots correspond to $q = 2$, the green dots correspond to $q = 3$, the red dots correspond to $q = 4$, and the purple dots correspond to $q = 5$.

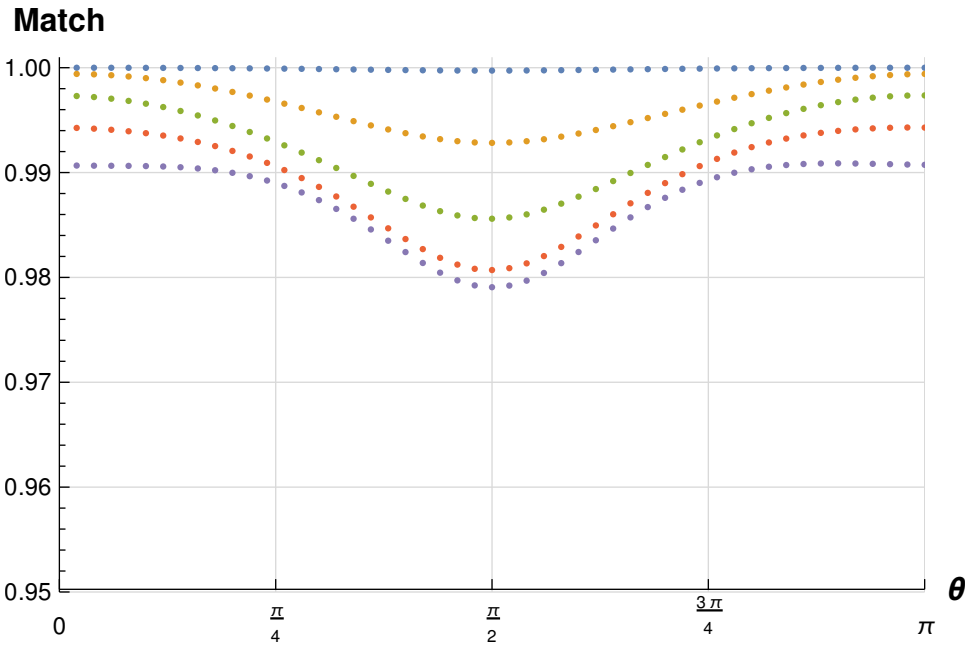

FIG. 5: The match between the $l = 2$ and $l = 4$ waveforms as a function of θ for a system with parallel spins. The blue dots correspond to $q = 1$, the orange dots correspond to $q = 2$, the green dots correspond to $q = 3$, the red dots correspond to $q = 4$, and the purple dots correspond to $q = 5$

V. NEXT STEPS

Now that we have calculated matches between quadrupole waveforms and full waveforms at various points in the parameter space by varying mass ratio, spin vectors, and inclination angle, we will perform the Fisher Matrix Analysis described in Sec. III A on binary cases that, according to our calculated matches,

have significant differences between their quadrupole waveform and their full waveform as we expect a correlation between the mismatch (i.e., $1-\mathscr{M}$) and the effect on parameter estimation. This will our first estimate of how the inclusion of higher modes in the inspiral waveform of low mass precessing black hole binaries affects parameter estimation.

Appendix A: Straight Line Fit Example

We performed an exercise where we generated a set of data points (x_i, y_i) of the form:

$$y_i = m_0 x_i + b_0 + n_i, \tag{A1}$$

where n_i was some Gaussian noise with zero mean. This is analogous to observing some signal y_i which contains a linear "signal", $h(x_i;\ m,\ b) = mx_i + b$, and some roughly Gaussian noise n_i. We estimated Gaussian noise by letting each n_i be a random real number in the interval $[-a, a]$, where a is the amplitude of the noise. Furthermore, each y_i data point has some uncertainty σ_i associated with it. Our goal is now to use a Fisher matrix analysis to determine the degree to which the presence of noise in our data effects the statistical uncertainty in recovering the m_0 and b_0 values used to generate the data.

The log-likelihood function of the data is found to be:

$$\ln[L(y_i|m,b)] = \sum_i \frac{mx_i + b - y_i}{(\sigma_i^2)}. \tag{A2}$$

As described in Section III A, we can then find the Fisher information matrix of the data by taking the second order gradient of the log-likelihood function. We did so using numerical finite differencing methods and inverted the resulting matrix to obtain the covariance matrix for the data points as a function of our estimated values m and b for the true values m_0 and b_0. The covariance matrix was thus a 2x2 matrix of the form:

$$\Gamma^{-1}(m,b) = \begin{pmatrix} \sigma_m^2 & \sigma_{mb} \\ \sigma_{bm} & \sigma_b^2 \end{pmatrix}, \tag{A3}$$

where σ_m and σ_b represent the standard deviation in m and b respectively, and $\sigma_{mb} = \sigma_{bm}$ is the correlation between the values of m and b. For a noise amplitude of $a = 0.2$ and $m = m_0 = 1$ and $b = b_0 = 2$, we get the following covariance matrix:

$$\Gamma^{-1}(1,2) = \begin{pmatrix} 0.304137 & -0.109558 \\ -0.109558 & 0.119344 \end{pmatrix}. \tag{A4}$$

From the covariance matrix, we want to construct the 1σ and 2σ confidence ellipses, which correspond to confidence levels of 68.3% and 95.4% respectively. The ellipse for each confidence level represents the region in which we can state that for repeated measurements, the probability that the true values m_0 and b_0 lie within the ellipse is given by the confidence level.

$$a^2 = \alpha^2 \left(\frac{\sigma_m^2 + \sigma_b^2}{2} + \sqrt{\frac{(\sigma_m^2 - \sigma_b^2)^2}{4} + \sigma_{mb}^2} \right), \tag{A5}$$

$$b^2 = \alpha^2 \left(\frac{\sigma_m^2 + \sigma_b^2}{2} - \sqrt{\frac{(\sigma_m^2 - \sigma_b^2)^2}{4} + \sigma_{mb}^2} \right), \tag{A6}$$

and

$$\tan(2\theta) = \frac{2\sigma_{mb}}{\sigma_m^2 - \sigma_b^2}, \tag{A7}$$

where a is the major axis of the ellipse, b is the minor axis of the ellipse, θ is the counterclockwise rotation of the ellipse, and α changes based on what confidence interval you want the ellipse to represent. For a 1σ, or 68.3%, confidence level, $\alpha = 1.52$. For a 2σ, or 95.4%, confidence level, $\alpha = 2.48$ [**?**].

Using this information, we can compute confidence ellipses for our estimated m and b values to see how the presence of noise effects how well our data constrains these parameters. We can do so for multiple noise amplitudes a to see how the shape and size of the confidence ellipses change for noisier data.

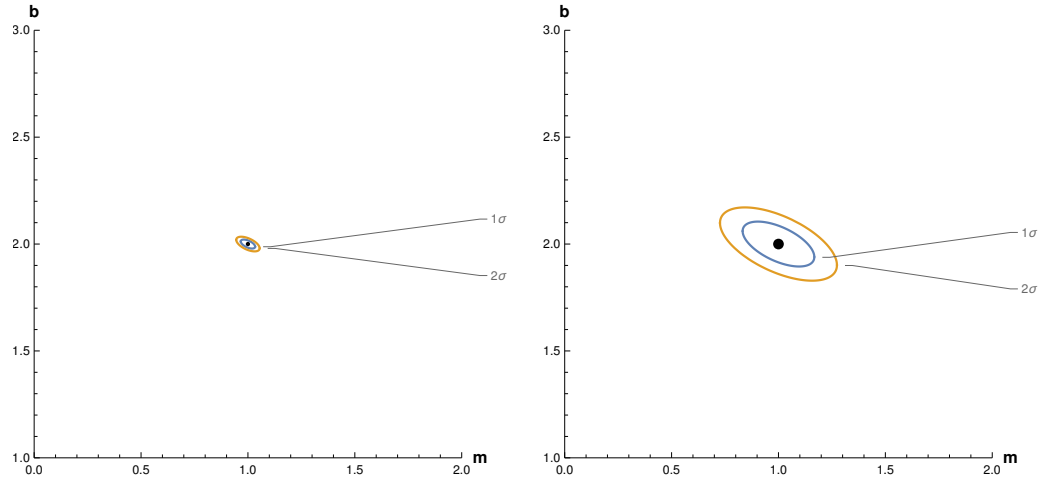

(a) $a = 0.2$ (b) $a = 1$

(c) $a = 3$ (d) $a = 5$

FIG. 6: Error ellipses for $m = m_0 = 1$ and $b = b_0 = 2$ at various noise amplitudes a. Blue ellipses are the 1σ confidence ellipses, and orange ellipses are the 2σ confidence ellipses.Patricia: The axis labels are too small.

From these figures, we are able to see that the tilt in the ellipse does not change with increasing noise, indicating that the correlation between m and b is independent of the level of noise. The only thing that appears to change as noise level increases is the overall area of the confidence ellipse, which indicates that as the noise level increases, the level to which the data is able to constrain the parameters m and b of the data decreases.

This exercise is an example of how one might use Fisher analysis on a set of data to determine the level of statistical error that is introduced to any parameter estimation by the presence of noise. Similarly, when analyzing the waveforms of our binary cases, we will need to use the methods shown above calculate the statistical error due to Gaussian noise that we can expect during parameter estimation. We will then compare our statistical error values to our systematic error values to determine whether or not our full waveforms are "indistinguishable" from our quadrupole and $\ell = 2$ waveforms, using the indistinguishability criterion outlined in Sec. III A.

---

[1] B. P. Abbott et al. Observation of Gravitational Waves from a Binary Black Hole Merger. *Phys. Rev. Lett.*, 116(6):061102, 2016.

[2] B. P. Abbott et al. Properties of the binary black hole merger GW150914. 2016.

[3] Emily Baird, Stephen Fairhurst, Mark Hannam, and Patricia Murphy. Degeneracy between mass and spin in black-hole-binary waveforms. *Phys. Rev.*, D87(2):024035, 2013.

[4] R. O'Shaughnessy, B. Farr, E. Ochsner, Hee-Suk Cho, C. Kim, and Chang-Hwan Lee. Parameter estimation of gravitational waves from nonprecessing black hole-neutron star inspirals with higher harmonics: Comparing Markov-chain Monte Carlo posteriors to an effective Fisher matrix. *Phys. Rev.*, D89(6):064048, 2014.

[5] Philip B. Graff, Alessandra Buonanno, and B.?S. Sathyaprakash. Missing Link: Bayesian detection and measurement of intermediate-mass black-hole binaries. *Phys. Rev.*, D92(2):022002, 2015.

[6] Emanuele Berti, Vitor Cardoso, Jose A. Gonzalez, Ulrich Sperhake, Mark Hannam, Sascha Husa, and Bernd Bruegmann. Inspiral, merger and ringdown of unequal mass black hole binaries: A Multipolar analysis. *Phys. Rev.*, D76:064034, 2007.

[7] R. O'Shaughnessy, Benjamin Farr, E. Ochsner, Hee-Suk Cho, V. Raymond, Chunglee Kim, and Chang-Hwan Lee. Parameter estimation of gravitational waves from precessing black hole-neutron star inspirals with higher harmonics. *Phys. Rev.*, D89(10):102005, 2014.

[8] Ilya Mandel, Christopher P. L. Berry, Frank Ohme, Stephen Fairhurst, and Will M. Farr. Parameter estimation on compact binary coalescences with abruptly terminating gravitational waveforms. *Class. Quant. Grav.*, 31:155005, 2014.

[9] Patricia Schmidt, Frank Ohme, and Mark Hannam. Towards models of gravitational waveforms from generic binaries: Ii. modelling precession effects with a single effective precession parameter. *Phys. Rev. D*, 91:024043, Jan 2015.

[10] Frank Ohme. *Bridging the Gap between Post-Newtonian Theory and Numerical Relativity in Gravitational-Wave Data Analysis*. PhD thesis, Potsdam, Max Planck Inst., 2012.

[11] Vijay Varma, Parameswaran Ajith, Sascha Husa, Juan Calderon Bustillo, Mark Hannam, and Michael Pürrer. Gravitational-wave observations of binary black holes: Effect of nonquadrupole modes. *Phys. Rev. D*, 90:124004, Dec 2014.

[12] J. Veitch et al. Parameter estimation for compact binaries with ground-based gravitational-wave observations using the LALInference software library. *Phys. Rev.*, D91(4):042003, 2015.

[13] The gravitational wave radiation field can be decomposed into spin weighted spherical harmonic modes, and, depending on the binary configuration, some modes may carry more energy than others. As a result, current template waveforms include only a few, dominant modes of the gravitational wave radiation field, in what is called the quadrupole approximation.